Reprinted from Applied Optics, Vol. 27 page 279, January 15, 1988

Optical constants for thin films of C, diamond, Al, Si, and CVD SiC from 24 Å to 1216 Å

David L. Windt, Webster C. Cash, Jr., M. Scott, P. Arendt, Brian Newnam, R. F. Fisher, A. B. Swartzlander, P. Z. Takacs, and J. M. Pinneo

A method for deriving optical constants from reflectance vs angle of incidence measurements using a nonlinear least-squares curve-fitting technique based on the χ^2 test of fit is presented and used to derive optical constants for several thin-film materials. The curve-fitting technique incorporates independently measured values for the film surface roughness, film thickness, and incident beam polarization. The technique also provides a direct method for estimating probable errors in the derived optical constants. Data are presented from 24 Å to 1216 Å for thin-film samples of C, synthetic diamond, Al, Si, and CVD SiC. Auger electron spectroscopy depth profiling measurements were performed on some of the samples to characterize sample composition including oxidation and contamination.

I. Introduction

The optical constants—the real and imaginary parts of the complex index of refraction—describe the optical properties of a given material; experimental data are needed for both optical instrumentation design and comparisons with solid-state theory. In the extreme ultraviolet and soft x rays ($10 \leq h\nu \leq 1000$ eV), specific applications include instrumentation for plasma physics, synchrotron radiation, space astronomy, and EUV and soft x-ray laser development, where the optical constants are needed to design optical coatings, multilayer reflectors, and bandpass filters.

Much of the optical data available in the literature in the present energy range was determined either from the use of isoreflectance curves using reflectance measurements made at two or more incidence angles, or from reflectance or transmittance measurements combined with Kramers-Kronig analysis. We present here a method for deriving optical constants from reflectance measurements made at multiple incidence angles using a nonlinear least-squares curve-fitting technique based on the χ^2 test of fit. Independently measured values for the sample surface roughness, sample thickness, and incident beam polarization are included in the curve-fitting procedure. In addition to deriving the best fit values for the optical constants, probable errors in these values are estimated by determining the region in parameter space for which an acceptable fit to the reflectance vs angle of incidence data can be achieved.

The present technique has been applied to measurements made on twenty-one thin-film samples. The data for samples of C, synthetic diamond, Al, Si, and CVD SiC are presented here along with Auger electron spectroscopy (AES) depth profiling measurements performed on some samples to characterize sample composition including oxidation and contamination. In a companion paper, we present similar data for thin film samples of Ti, Zr, Nb, Mo, Ru, Rh, Pd, Ag, Hf, Ta, W, Re, Os, Ir, Pt, and Au.

In Sec. II, the experimental techniques are presented, including sample preparation, reflectance measurements, surface roughness measurements, polarization measurements, and AES measurements. The data reduction techniques used to derive the optical constants are presented in Sec. III. Finally, in Sec. IV, the optical data are presented for the five samples measured in this work.

J. M. Pinneo is with Crystallume, Inc., Palo Alto, California 94304; P. Z. Takacs is with Brookhaven National Laboratory, Upton, New York 11973; R. F. Fisher and A. B. Swartzlander are with Solar Energy Research Institute, Golden, Colorado 804011; D. L. Windt and W. C. Cash, Jr., are with University of Colorado, Center for Astrophysics & Space Astronomy, Boulder, Colorado 80309; and the other authors are with Los Alamos National Laboratory, Materials Science & Technology Division, Los Alamos, New Mexico 87545.

Received 28 July 1987.
0003-6935/88/020279-17$02.00/0.

II. Experiment

A. Sample Preparation

Thin-film samples of C, Si, and Al were prepared in the coating facility of the Materials Science and Technology Division at the Los Alamos National Laboratory (LANL). The films were deposited using electron-beam evaporation onto polished 7.6-cm (3-in.) diam Si {111} wafers at room temperature in a vacuum of $\sim 5 \times 10^{-6}$ Torr. The film thickness was chosen to be 1000 Å and measured with a calibrated quartz crystal monitor. The SiC sample was an α-SiC substrate supplied by the Carborundum Corp. coated with chemical vapor deposited silicon carbide (CVD SiC) by the Research Division of the Raytheon Co. and then polished by Frank Cooke, Inc. The diamond film was provided by Crystallume, Inc., and was prepared onto a polished 5-cm (2-in.) diam Si {100} wafer using a variation of the electron-assisted CVD technique described by Sawabe and Inuzuka,[1] where electron bombardment is achieved from a glow discharge rather than a hot filament. All samples were sent to the University of Colorado for reflectance measurements.

B. Reflectance Measurements

Reflectance measurements were performed using a computer-controlled reflectometer that has been described previously.[2,3] The absolute reflectance at a particular incidence angle is measured by determining the ratio of the reflected intensity to the incident beam intensity; both measurements are made with the same detector, which is free to rotate about the sample from near-normal incidence to grazing incidence.

The samples are transferred in air to the reflectometer, and reflectance measurements are performed at several incidence angles. The light sources used in combination with a grazing incidence monochromator provide line emission from 24 Å to 1216 Å. A total of thirty-six wavelengths was chosen for the measurements presented here. For wavelengths >200 Å, reflectance measurements were typically made at sixteen incidence angles, from 5° to 80° in 5° increments. For wavelengths <200 Å, measurements were usually made at ten or more grazing angles. The computer-controlled sample manipulator positions the sample with a precision of 0.001° and with an absolute accuracy of 0.02°. Two detectors—an imaging microchannel plate and a gas proportional counter—are used for the EUV and soft x-ray wavelengths, respectively. The entire data acquisition process is controlled by an HP 9845B computer, and data are finally transferred to a VAX 8600 for processing. The reflectance vs incidence angle measurements for all thirty-six wavelengths typically take two to three days per sample.

C. Surface Roughness Measurements

Surface roughness reduces the amount of light reflected in the specular direction. In the determination of optical constants presented here, the effect of surface roughness is accounted for by the inclusion of a Debye-Waller factor in the Fresnel equations, as described in Sec. III. We assume that the distribution of surface heights can be characterized by an rms surface height σ. The value of σ for each sample was measured at several points on the surface using a WYKO optical profilometer[4] with a 10× objective. These measurements were used to determine a mean value and standard deviation for σ. The value of σ for the samples measured here was typically of the order of 15 Å ± 3 Å.

D. Polarization Measurements

The measured reflectance also depends on the incident beam polarization. The polarization of the beam used for the present work was measured using a rhodium mirror as a polarization analyzer in a method similar to that described by Rabinovitch *et al.*[5] The sample manipulator was reconfigured so that the Rh mirror could be positioned at a fixed incidence angle of 45° yet could be rotated about the incident beam. Thus the plane of incidence with respect to the laboratory frame could be varied continuously from horizontal to vertical. The microchannel plate detector was mounted on the manipulator so as to measure the intensity of light reflected from the analyzer for any orientation of the plane of incidence.

Since the grooves of the grating in the monochromator are parallel to the vertical, we expect the beam to be partially polarized in this direction. Thus the intensity of light reflected from the analyzer should decrease as the plane of incidence begins to coincide with the vertical direction, as the analyzer preferentially reflects light whose electric vector is perpendicular to the plane of incidence.

This effect can be understood by evaluating the reflectance of a mirror as measured with partially polarized light. We assume that the incident beam is partially plane polarized. We can then write the intensity of the beam as the sum of a polarized part and an unpolarized part[6]:

$$I_{\text{inc}} = I_{\text{pol}} + I_{\text{unpol}}. \tag{1}$$

We define the polarization fraction f as

$$f \equiv \frac{I_{\text{pol}}}{I_{\text{inc}}}, \tag{2}$$

and we assume further that the plane-polarized part of the beam has its electric field vector oriented at an angle ϕ with respect to the vertical direction. We take the s direction to be perpendicular to the plane of incidence and the p direction parallel to the plane of incidence. It can be shown that the measured reflectance would then be given by

$$R = \frac{R_p}{2} \cdot (1 - f\cos 2\phi) + \frac{R_s}{2} \cdot (1 + f\cos 2\phi), \tag{3}$$

where R_p and R_s are the reflectances for pure p and s polarizations, respectively. The quantities R_p and R_s are characteristic of the mirror. For the polarization measurements described here, we assume[7] values for R_p and R_s based on the optical constants for Rh from Palik.[8]

When the plane of incidence is horizontal, the s direction is parallel to the vertical. When the analyzer is rotated by an angle β, the s and p axes also rotate with respect to the laboratory frame by the same angle β, and hence ϕ in Eq. (3) must be replaced by the quantity $\beta + \phi$. We thus write the reflectance as a function of β as

$$R(\beta) = \frac{R_p}{2} \cdot [1 - f\cos 2(\phi + \beta)] + \frac{R_s}{2} \cdot [1 + f\cos 2(\phi + \beta)]. \quad (4)$$

By measuring the reflectance of the analyzer for three or more orientations β, we can deduce the value of the quantity $f\cos 2\phi$. We determine the relative reflectance $P(\beta)$—the ratio of the reflectance measured at an angle β to the reflectance at $\beta = 0$—for two or more angles β. The quantity $P(\beta)$ is given by

$$P(\beta) \equiv \frac{R(\beta)}{R(\beta = 0)} = \frac{\frac{R_p}{2} \cdot [1 - f\cos 2(\phi + \beta)] + \frac{R_s}{2} \cdot [1 + f\cos 2(\phi + \beta)]}{\frac{R_p}{2} \cdot (1 - f\cos 2\phi) + \frac{R_s}{2} \cdot (1 + f\cos 2\phi)} \quad (5)$$

$$= \frac{\left(1 + \frac{R_p}{R_s}\right) + f\cos 2(\phi + \beta) \cdot \left(1 - \frac{R_p}{R_s}\right)}{\left(1 + \frac{R_p}{R_s}\right) + f\cos 2\phi \cdot \left(1 - \frac{R_p}{R_s}\right)}. \quad (6)$$

The relative reflectance of the analyzer was measured for several rotation angles for wavelengths >200 Å used for reflectance measurements. The analyzer was oriented at seven angles β from 0 to 90° in 15° increments, and the curve-fitting technique described in the next section was used to deduce the value of the quantity $F \equiv f\cos 2\phi$ as a function of wavelength by fitting Eq. (6) to the measured reflectance vs rotation angle curves. A typical curve of relative reflected intensity vs rotation angle is shown in Fig. 1. The derived value of F as a function of wavelength is shown in Fig. 2. The probable errors in the measured values of F are shown as the vertical lines.

For wavelengths >200 Å the function $F(\lambda)$ was approximated by a straight line of the form

$$F(\lambda) = a_0 + a_1 \cdot \lambda. \quad (7)$$

The best fit values of the coefficients in this equation were found to be $a_0 = -0.0412$, $a_1 = 2.087 \times 10^{-4}$. It is this equation that is used to estimate the polarization F for wavelengths >200 Å in the determination of the optical constants, as described in the next section. The uncertainty in F is taken to be ±0.01 and is shown as the dotted lines in Fig. 2. The probable errors in the measured values of F have perhaps been overestimated. The reason for this overestimation is not clear.

For wavelengths of <200 Å, the polarization is taken to be zero. This is justified by the fact that the grating in the monochromator is used at very small grazing angles for these wavelengths, and hence the beam is less likely to be significantly polarized. Furthermore, the reflectance measurements for these wavelengths were typically made at large incidence angles. The difference between the reflectances for s and p polarizations is smaller for larger incidence angles so the incident beam polarization has a diminished effect on the determination of the optical constants.

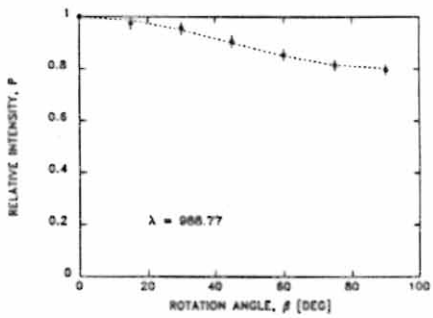

Fig. 1. Typical curve of relative reflected intensity vs rotation angle used to determine the incident beam polarization. Shown are the data for 989 Å.

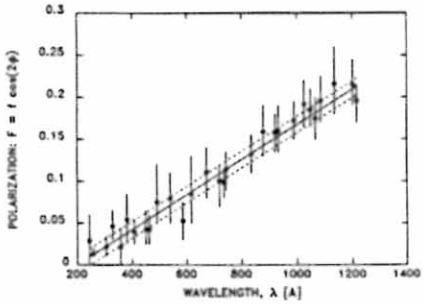

Fig. 2. Polarization $F = f\cos 2\phi$ as a function of wavelength. Also shown is the straight line fit, $F = -0.0412 + \lambda \cdot 2.087 \times 10^{-4}$ (solid line). The error to this fit is taken to be ±0.01, represented by the dotted lines.

D. Auger Electron Spectroscopy Measurements

Sample purity and the presence of overlayers can significantly affect the optical properties of materials in the present energy range. The samples measured in this work were all exposed to air before reflectance measurements. In addition, the e-beam evaporated samples were prepared in a vacuum of $\sim 5 \times 10^{-6}$ Torr. Some of the samples are, therefore, likely to be oxidized and/or contaminated. To characterize sample composition, Auger electron spectroscopy (AES) depth profiling measurements were performed for the C, Si, and Al samples.

The AES measurements were performed at the Solar Energy Research Institute using a Physical Electronics Industries model PHI 600 scanning auger microprobe. The incident electron energy was 5 keV, and etching was achieved with 3 keV Ar^+ ions. In Sec. IV, we present along with the optical data the resulting plots of the peak-to-peak Auger signals vs sputtering time.

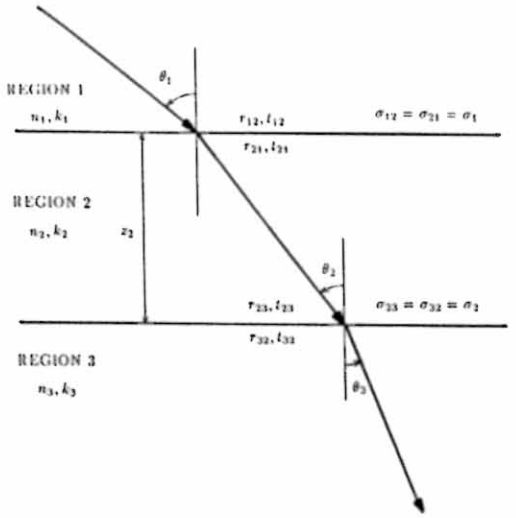

Fig. 3. Three-phase optical system.

III. Data Reduction

The objective of the data reduction scheme is to derive the values of the optical constants for which the calculated reflectance (Ref) most closely fits the measured reflectance $R \pm \delta R$ for all incidence angles θ_i. As a measure of closeness of fit we use the χ^2 test.[9] That is, we compute the value of the statistic S, defined as

$$S \equiv \sum_{i=1}^{N} \frac{[R_i - \mathrm{Ref}(\theta_i)]^2}{(\delta R_i)^2} . \tag{8}$$

It can be shown[10] that the minimum value found $S_{\min}$ is distributed as the χ^2 probability function with $(N-p)$ degrees of freedom. We can thus determine the significance of the fit α by equating

$$S_{\min} = \chi^2_{N-p}(\alpha), \tag{9}$$

where the quantity $\chi^2_{N-p}(\alpha)$ is the tabulated value of the χ^2 function with significance α. We may then vary the p adjustable parameters in the model for reflectance so as to minimize S and hence deduce the best fit values for the adjustable parameters.

A. Modeling Reflectance

We calculate the reflectance for a three-phase model, which consists of a substrate, thin film and ambient medium (vacuum), as shown in Fig. 3. The optical properties in the three regions are contained in the optical constants n and k, which are the real and imaginary parts of the complex index of refraction. Thus the optical properties of regions 1, 2, and 3 are contained in the complex indices of refraction $\mathbf{n}_1 = 1$, $\mathbf{n}_2 = n_2 + ik_2$, and $\mathbf{n}_3 = n_3 + ik_3$, respectively. We suppose that light is incident in region 1 with incidence angle θ_1 measured from the normal and propagates in region 2 with angle θ_2 and in region 3 with angle θ_3. The angles are determined in each region from Snell's law:

$$\mathbf{n}_1 \sin\theta_1 = \mathbf{n}_2 \sin\theta_2 = \mathbf{n}_3 \sin\theta_3. \tag{10}$$

The overall reflection coefficient for the three-phase system is given in terms of the Fresnel coefficients at each interface:

$$r = r_{12} + \frac{r_{23} t_{12} t_{21} \exp(2i\beta)}{1 + r_{12} r_{23} \exp(2i\beta)} , \tag{11}$$

where

$$\beta \equiv \frac{2\pi \mathbf{n}_2 z \cos\theta_2}{\lambda} . \tag{12}$$

The quantity z is the thickness of the film, and λ is the wavelength of light. The Fresnel reflection and transmission coefficients for the interface between two regions i and j are

$$r^s_{ij} = \left(\frac{\mathbf{n}_i \cos\theta_i - \mathbf{n}_j \cos\theta_j}{\mathbf{n}_i \cos\theta_i + \mathbf{n}_j \cos\theta_j}\right) \exp\left[-2\left(\frac{2\pi\sigma_{ij}\cos\theta_i}{\lambda}\right)^2\right], \tag{13}$$

$$t^s_{ij} = \frac{2\mathbf{n}_i \cos\theta_i}{\mathbf{n}_i \cos\theta_i + \mathbf{n}_j \cos\theta_j} , \tag{14}$$

for s polarization, and

$$r^p_{ij} = \left(\frac{\mathbf{n}_i \cos\theta_j - \mathbf{n}_j \cos\theta_i}{\mathbf{n}_i \cos\theta_j + \mathbf{n}_j \cos\theta_i}\right) \exp\left[-2\left(\frac{2\pi\sigma_{ij}\cos\theta_i}{\lambda}\right)^2\right], \tag{15}$$

$$t^p_{ij} = \frac{2\mathbf{n}_i \cos\theta_i}{\mathbf{n}_i \cos\theta_j + \mathbf{n}_j \cos\theta_i} , \tag{16}$$

for p polarization. It is these quantities, evaluated at each interface, that are used in Eq. (11) to calculate the reflectance. The exponentials in Eqs. (13) and (15) are Debye-Waller factors used to account for the loss in reflectance due to surface roughness scattering. In the simple model for surface roughness used here, it is assumed that at each interface the distribution of surface heights is Gaussian and can be described by an rms surface height parameter σ; the surface height at the top interface is $\sigma_{12} = \sigma_{21} \equiv \sigma_1$, and at the bottom interface it is $\sigma_{23} = \sigma_{32} \equiv \sigma_2$.

The net reflectance for such a system, as measured with partially polarized light, is then

$$\mathrm{Ref} = \frac{R_p}{2} \cdot (1 - F) + \frac{R_s}{2} \cdot (1 + F), \tag{17}$$

where $F \equiv f \cos 2\phi$ is the incident beam polarization. The quantities R_p and R_s are the reflectances for pure p and s polarizations, respectively, defined as the squares of the magnitudes of the overall reflection coefficients [Eq. (11) using the Fresnel coefficients corresponding to the appropriate polarizations].

B. Curve-Fitting Procedure

We now have a model for reflectance that depends on the quantities n_2, k_2, n_3, k_3, z, σ_1, σ_2, F, and θ. We take θ to be the independent variable and consider the remaining eight variables as adjustable parameters. The objective is to determine just two of these parameters, n_2 and k_2, which are the optical constants of the film.

We determine the best fit values for n_2 and k_2 by varying these quantities so as to minimize the S statistic defined by Eq. (8). We can fix the values of the other six adjustable parameters: For the e-beam

evaporated films, we take the measured value of the film thickness: $z = 1000$ Å. For the diamond and SiC samples, we assume $z = 2500$ Å, which is an underestimate but nonetheless large enough so that the films are optically opaque for the present energy range. We assume that $\sigma_1 = \sigma_2 \equiv \sigma$, where σ is the value of the rms surface height as determined from the WYKO measurements described above. We use Eq. (7) to evaluate the polarization of the incident beam F. The parameters n_3 and k_3—the optical constants of the substrate—are fixed to the values for crystalline silicon from Palik[8] (except for the SiC sample, where we take the values of SiC from Palik, as this sample was prepared on a SiC substrate). It was found that the choice of substrate optical constants has essentially no effect on the outcome of the derivation of the best fit values for n_2 and k_2. This was determined by deriving n_2 and k_2 (as described below) for values of n_3 and k_3 ranging from 50 to 150% of the values for silicon from Palik. Thus, even though the e-beam deposited samples are not completely opaque, the calculated reflectance is relatively insensitive to changes in the substrate optical constants.

Using the Curvefit algorithm described by Bevington,[9] we determine the best fit values of n_2 and k_2 by searching the $n_2 - k_2$ parameter space until we find the values for which the statistic S is at a minimum. The optical constants were determined in this way on a VAX 8600 computer, typically using no more than 30 s of CPU time per wavelength. The time used depends in part on the initial values of the free parameters; if the derived values of n_2 and k_2 are much different from the initial values, the algorithm requires more iterations and hence more computation time until the best fit is obtained. Optical data available in the literature were used to infer initial values for the materials measured here. An example of the measured reflectance vs incidence angle is shown in Fig. 4, along with the fit to this curve.

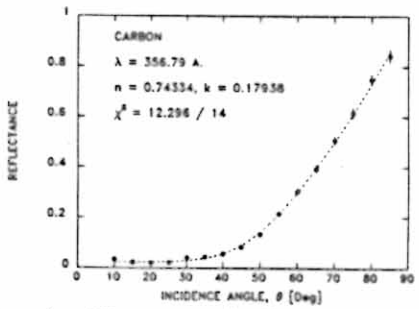

Fig. 4. Example of the measured reflectance vs incidence angle taken from the results for C at 357 Å. The data are shown as circles with 1σ error bars (vertical lines). The fit to this curve is the dashed line. The derived values of n and k are indicated. The next line is the value of the χ^2 statistic S and the number of degrees of freedom $N - p$ (= number of data points—number of free parameters = 14, in this case) expressed as $S/(N - p)$.

C. Error Analysis

The best fit values of n_2 and k_2 (those corresponding to $S_{\min}$) are not the only ones for which an acceptable fit can be found. Thus to estimate the probable errors in the derived optical constants, we determine the region in $n_2 - k_2$ parameter space in which we can say that the true values of n_2 and k_2 lie with some specific probability. We call this region the joint confidence interval.

We calculate the joint confidence interval[10] by evaluating the S statistic throughout parameter space and determine the region for which S is less than some limiting value S_L. Thus the confidence interval is given by the region where

$$S < S_L, \tag{18}$$

where we take

$$S_L = S_{\min} + \Delta S(\alpha). \tag{19}$$

Lampton *et al.*[10] have shown that the quantity $\Delta S(\alpha)$ is distributed as χ^2 with p degrees of freedom, where p is the number of parameters that were varied to minimize S. Thus, if $\Delta S(\alpha)$ is equal to the tabulated value of the χ^2 function with p degrees of freedom and significance α, the resulting p-dimensional confidence region (that region for which $S < S_L$) will enclose the true values of the p parameters in $1 - \alpha$ of all experiments. For example, if we take $\Delta S = 2.3$ for a model with two free parameters, we can say that the probability is 68% that the resulting confidence region contains the true values of the two parameters, since $\Delta S = 2.3 = \chi_2^2(\alpha = 0.32)$, and so $1 - \alpha = 0.68$.

Joint confidence intervals were determined by constructing a grid of points in $n_2 - k_2$ parameter space and evaluating the S statistic at each point on the grid. Additionally, the experimental uncertainties in the adjustable parameters z, σ, and F (which were fixed to their measured values in the determination of the best fit values of the optical constants) were included in the estimation of the errors in n_2 and k_2. This was achieved by minimizing S at each point on the grid in $n_2 - k_2$ parameter space by varying each of these parameters through their respective ranges of uncertainty. This has the effect of increasing the size of the confidence intervals.

An example of a confidence contour determined in this way is shown in Fig. 5. The solid line indicates the 68% joint confidence interval on n_2 and k_2, corresponding to $\Delta S = 2.3$.

Although the joint confidence interval has the most meaning, it is in fact the independent confidence intervals on n_2 and k_2 that will be the most useful. Confidence intervals for single parameters can be determined again by evaluating the parameter range for which $S < S_L$, except we now take ΔS to be the tabulated value of the χ^2 function for one degree of freedom. Thus the 68% independent confidence interval corresponds to $\Delta S = 1 = \chi_1^2(\alpha = 0.32)$. This is shown in Fig. 5 as the dotted line region. We can thus determine '1σ' errors on n_2 and k_2 by observing the extent of the 68% independent confidence interval along the n_2 and k_2 axes, respectively.

Table I. Optical Constants for Carbon

Wavelength (Å)	Index of refraction n		Extinction coefficient k	
23.6	0.99831	(0.99830, 0.99845)	0.000503	(0.000450, 0.000550)
31.6	0.99831	(0.99820, 0.99840)	0.000493	(0.000400, 0.000600)
67.6	0.99194	(0.99190, 0.99200)	0.000729	(0.000700, 0.000850)
114.0	0.9742	(0.9740, 0.9750)	0.00411	(0.00350, 0.00480)
135.5	0.9633	(0.9630, 0.9640)	0.00529	(0.00480, 0.00650)
171.4	0.9280	(0.9275, 0.9285)	0.0155	(0.0150, 0.0160)
243.0	0.870	(0.869, 0.878)	0.0499	(0.0440, 0.0500)
256.3	0.863	(0.863, 0.870)	0.0538	(0.0480, 0.0550)
303.8	0.811	(0.810, 0.818)	0.0969	(0.0920, 0.0970)
327.0	0.774	(0.760, 0.785)	0.146	(0.135, 0.160)
356.8	0.743	(0.742, 0.758)	0.179	(0.163, 0.184)
379.3	0.728	(0.725, 0.740)	0.196	(0.180, 0.200)
405.9	0.693	(0.675, 0.695)	0.245	(0.240, 0.265)
447.8	0.654	(0.635, 0.664)	0.346	(0.320, 0.380)
460.7	0.633	(0.615, 0.640)	0.375	(0.370, 0.405)
489.5	0.651	(0.635, 0.665)	0.439	(0.420, 0.450)
539.1	0.617	(0.605, 0.625)	0.558	(0.525, 0.610)
584.3	0.651	(0.640, 0.665)	0.751	(0.710, 0.800)
616.3	0.714	(0.690, 0.740)	0.796	(0.740, 0.860)
671.4	0.763	(0.725, 0.790)	0.967	(0.900, 1.00)
718.5	0.912	(0.880, 1.00)	1.09	(1.04, 1.20)
735.9	0.915	(0.850, 0.980)	1.10	(1.02, 1.17)
743.7	0.997	(0.940, 1.03)	1.16	(1.10, 1.22)
834.5	1.13	(1.10, 1.22)	1.18	(1.16, 1.24)
878.0	1.47	(1.38, 1.62)	1.24	(1.20, 1.28)
919.8	1.43	(1.30, 1.52)	1.21	(1.17, 1.25)
932.1	1.42	(1.34, 1.58)	1.16	(1.13, 1.20)
988.8	1.41	(1.33, 1.53)	1.10	(1.07, 1.12)
1025.8	1.45	(1.38, 1.60)	1.00	(0.980, 1.02)
1048.2	1.70	(1.62, 1.80)	0.978	(0.940, 1.01)
1066.7	1.71	(1.62, 1.84)	0.937	(0.880, 0.970)
1085.7	1.75	(1.63, 1.90)	0.859	(0.820, 0.910)
1135.0	1.87	(1.72, 2.02)	0.708	(0.570, 0.800)
1200.7	1.71	(1.63, 1.87)	0.691	(0.600, 0.730)
1215.7	1.77	(1.68, 1.91)	0.663	(0.530, 0.720)

Table II. Optical Constants for Synthetic Diamond Film

Wavelength (Å)	Index of refraction n		Extinction coefficient k	
243.0	0.9162	(0.9145, 0.9175)	0.0731	(0.0700, 0.0770)
256.3	0.9137	(0.9135, 0.9140)	0.0656	(0.0645, 0.0660)
303.8	0.880	(0.878, 0.882)	0.107	(0.103, 0.110)
327.0	0.870	(0.868, 0.872)	0.122	(0.117, 0.127)
356.8	0.864	(0.863, 0.865)	0.141	(0.133, 0.148)
379.3	0.857	(0.857, 0.858)	0.159	(0.150, 0.168)
405.9	0.853	(0.852, 0.854)	0.180	(0.170, 0.185)
447.8	0.844	(0.842, 0.845)	0.186	(0.168, 0.190)
460.7	0.831	(0.830, 0.833)	0.186	(0.182, 0.192)
489.5	0.843	(0.842, 0.844)	0.200	(0.185, 0.215)
539.1	0.828	(0.825, 0.832)	0.295	(0.280, 0.308)
584.3	0.786	(0.785, 0.787)	0.273	(0.268, 0.275)
616.3	0.799	(0.793, 0.808)	0.376	(0.350, 0.400)
671.4	0.785	(0.780, 0.788)	0.388	(0.363, 0.400)
718.5	0.807	(0.805, 0.813)	0.453	(0.442, 0.465)
735.9	0.825	(0.823, 0.828)	0.498	(0.490, 0.510)
743.7	0.840	(0.838, 0.850)	0.500	(0.490, 0.505)
834.5	0.881	(0.875, 0.900)	0.602	(0.595, 0.620)
878.0	0.947	(0.930, 0.980)	0.653	(0.640, 0.670)
919.8	0.969	(0.960, 0.980)	0.693	(0.685, 0.705)
932.1	1.06	(1.05, 1.10)	0.734	(0.720, 0.750)
988.8	1.15	(1.12, 1.22)	0.789	(0.780, 0.800)
1025.8	1.13	(1.08, 1.20)	0.762	(0.740, 0.783)
1048.2	1.23	(1.20, 1.30)	0.823	(0.815, 0.825)
1066.7	1.24	(1.20, 1.33)	0.799	(0.780, 0.800)
1085.7	1.25	(1.20, 1.35)	0.698	(0.690, 0.705)
1135.0	1.47	(1.40, 1.60)	0.640	(0.590, 0.660)
1200.7	1.25	(1.20, 1.35)	0.648	(0.638, 0.655)
1215.7	1.17	(1.15, 1.23)	0.619	(0.610, 0.623)

Table III. Optical Constants for Aluminum

Wavelength (Å)	Index of refraction n		Extinction coefficient k	
23.6	0.99828	(0.99824, 0.99829)	0.000197	(0.000148, 0.000198)
31.6	0.99777	(0.99775, 0.99795)	0.000558	(0.000400, 0.000700)
44.7	0.99344	(0.99343, 0.99345)	0.00206	(0.00195, 0.00210)
67.6	0.99676	(0.98600, 0.98750)	0.00778	(0.00750, 0.00800)
114.0	0.9832	(0.9805, 0.9880)	0.0381	(0.0300, 0.0550)
135.5	0.9851	(0.9830, 0.992)	0.0432	(0.0380, 0.0560)
171.4	1.04	(1.02, 1.05)	0.0159	(0.0150, 0.0350)
243.0	0.9698	(0.9697, 0.9702)	0.00895	(0.00870, 0.00980)
256.3	0.9640	(0.9638, 0.9650)	0.0116	(0.0110, 0.0122)
303.8	0.9490	(0.9483, 0.9493)	0.0150	(0.0148, 0.0152)
327.0	0.9377	(0.9363, 0.9386)	0.0203	(0.0195, 0.0210)
356.8	0.9293	(0.9278, 0.9302)	0.0221	(0.0205, 0.0235)
379.3	0.9144	(0.9120, 0.9160)	0.0307	(0.0290, 0.0323)
405.9	0.9068	(0.9048, 0.9070)	0.0281	(0.0275, 0.0290)
447.8	0.883	(0.880, 0.884)	0.0412	(0.0410, 0.0420)
460.7	0.851	(0.847, 0.855)	0.0634	(0.0600, 0.0670)
489.5	0.857	(0.853, 0.858)	0.0530	(0.0520, 0.0550)
539.1	0.822	(0.817, 0.823)	0.0822	(0.0780, 0.0870)
584.3	0.796	(0.792, 0.797)	0.0959	(0.0940, 0.1000)
616.3	0.767	(0.760, 0.772)	0.131	(0.122, 0.140)
671.4	0.723	(0.715, 0.728)	0.191	(0.180, 0.200)
718.5	0.699	(0.695, 0.705)	0.277	(0.260, 0.300)
735.9	0.681	(0.678, 0.682)	0.286	(0.265, 0.300)
743.7	0.678	(0.678, 0.682)	0.288	(0.270, 0.300)
834.5	0.670	(0.668, 0.678)	0.391	(0.375, 0.415)
878.0	0.660	(0.658, 0.663)	0.397	(0.380, 0.420)
919.8	0.677	(0.675, 0.680)	0.423	(0.405, 0.440)
932.1	0.680	(0.670, 0.690)	0.463	(0.440, 0.480)
988.8	0.684	(0.675, 0.690)	0.468	(0.450, 0.482)
1025.8	0.658	(0.650, 0.668)	0.481	(0.453, 0.505)
1048.2	0.691	(0.680, 0.700)	0.585	(0.580, 0.600)
1066.7	0.720	(0.709, 0.740)	0.649	(0.628, 0.680)
1085.7	0.671	(0.660, 0.683)	0.570	(0.540, 0.600)
1135.0	0.626	(0.610, 0.643)	0.659	(0.620, 0.700)
1200.7	0.585	(0.568, 0.620)	0.747	(0.705, 0.800)
1215.7	0.607	(0.590, 0.640)	0.855	(0.810, 0.900)

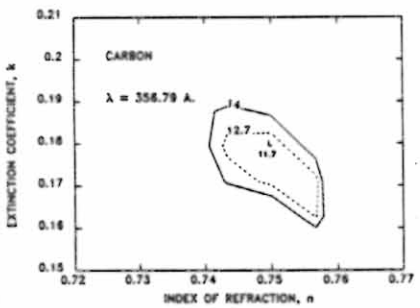

Fig. 5. Typical confidence interval on n_2 and k_2. Shown is the contour for C at 357 Å. The solid line corresponds to a $\Delta S(\alpha)$ of 2.3 and the dotted line a value of 1. The solid line, therefore, represents the 68% joint confidence on n_2 and k_2 (two degrees of freedom; $\alpha = 0.32$). The dotted line is used to estimate the 68% confidence limits on n_2 and k_2 independently, since a $\Delta S(\alpha) = 1$ corresponds to the value of the χ^2 function with one degree of freedom for $\alpha = 0.32$.

Confidence regions, and hence probable errors on the derived values of n and k, were determined in this way for each wavelength and each sample measured, typically using ~90 s of CPU time on the VAX 8600. The results of these calculations are presented in Sec. IV as '1σ' errors in n and k.

D. Effect of Surface Roughness

Before presenting the results of the measurements and data reduction techniques just described, we discuss the sensitivity of the derived optical constants to the assumed value of σ used in the derivation.

Surface roughness has the effect of reducing the amount of light reflected in the specular direction. This reduction in reflectance is accounted for in this work by including a Debye-Waller factor in the Fresnel reflection coefficients, where we assume that the surface roughness can be described by an rms surface height σ. In the determination of the optical constants from reflectance measurements, the value of σ is fixed to the value determined from the WYKO optical profilometer measurements described above.

To see how strongly the derived n and k depend on the value of σ used, the optical constants were derived using two different values of σ, for three arbitrarily chosen samples out of the twenty-one thin-film samples that have thus far been measured using the apparatus and techniques described above. The samples that were considered are thin films of Nb, Hf, and Os; the optical constants for these samples are not in fact presented in this paper but in a companion paper.[11]

Table IV. Optical Constants for Silicon

Wavelength (Å)	Index of refraction n		Extinction coefficient k	
23.6	0.99875	(0.99870, 0.99876)	0.000352	(0.000320, 0.000380)
31.6	0.99826	(0.99825, 0.99831)	0.000673	(0.000620, 0.000680)
44.7	0.99524	(0.99520, 0.99545)	0.00211	(0.00200, 0.00215)
67.6	0.99058	(0.99056, 0.99100)	0.00772	(0.00700, 0.00780)
114.0	0.9938	(0.9928, 0.9950)	0.0196	(0.0175, 0.0220)
135.5	0.9857	(0.9856, 0.9862)	0.0060	(0.0055, 0.0065)
171.4	0.9617	(0.9000, 0.9620)	0.0195	(0.0190, 0.0200)
243.0	0.9439	(0.9430, 0.9453)	0.0336	(0.0310, 0.0350)
256.3	0.9433	(0.9430, 0.9440)	0.0301	(0.0290, 0.0320)
303.8	0.9234	(0.9218, 0.9250)	0.0487	(0.0460, 0.0520)
327.0	0.9144	(0.9140, 0.9150)	0.0531	(0.0500, 0.0570)
356.8	0.9010	(0.9000, 0.9040)	0.0620	(0.0557, 0.0650)
379.3	0.890	(0.887, 0.894)	0.0758	(0.0700, 0.0800)
405.9	0.877	(0.875, 0.880)	0.0785	(0.0720, 0.0830)
447.8	0.854	(0.848, 0.855)	0.0985	(0.0980, 0.105)
460.7	0.839	(0.838, 0.840)	0.112	(0.110, 0.115)
489.5	0.833	(0.832, 0.834)	0.130	(0.128, 0.132)
539.1	0.802	(0.800, 0.804)	0.180	(0.173, 0.187)
584.3	0.781	(0.776, 0.782)	0.209	(0.208, 0.218)
616.3	0.790	(0.786, 0.794)	0.275	(0.260, 0.290)
671.4	0.810	(0.803, 0.820)	0.331	(0.310, 0.360)
718.5	0.801	(0.788, 0.820)	0.453	(0.430, 0.480)
735.9	0.788	(0.780, 0.800)	0.422	(0.410, 0.440)
743.7	0.811	(0.800, 0.830)	0.460	(0.440, 0.480)
834.5	0.849	(0.835, 0.870)	0.567	(0.548, 0.590)
878.0	0.848	(0.830, 0.870)	0.566	(0.550, 0.600)
919.8	0.925	(0.908, 0.960)	0.646	(0.630, 0.668)
932.1	0.933	(0.900, 0.970)	0.656	(0.630, 0.680)
988.8	1.02	(0.990, 1.06)	0.707	(0.690, 0.730)
1025.8	1.02	(0.990, 1.06)	0.705	(0.685, 0.730)
1048.2	1.00	(0.980, 1.05)	0.715	(0.700, 0.730)
1066.7	1.05	(1.03, 1.10)	0.732	(0.720, 0.750)
1085.7	0.980	(0.960, 1.03)	0.707	(0.680, 0.730)
1135.0	1.09	(1.05, 1.15)	0.784	(0.765, 0.810)
1200.7	1.09	(1.05, 1.15)	0.805	(0.780, 0.830)
1215.7	1.12	(1.07, 1.18)	0.845	(0.820, 0.870)

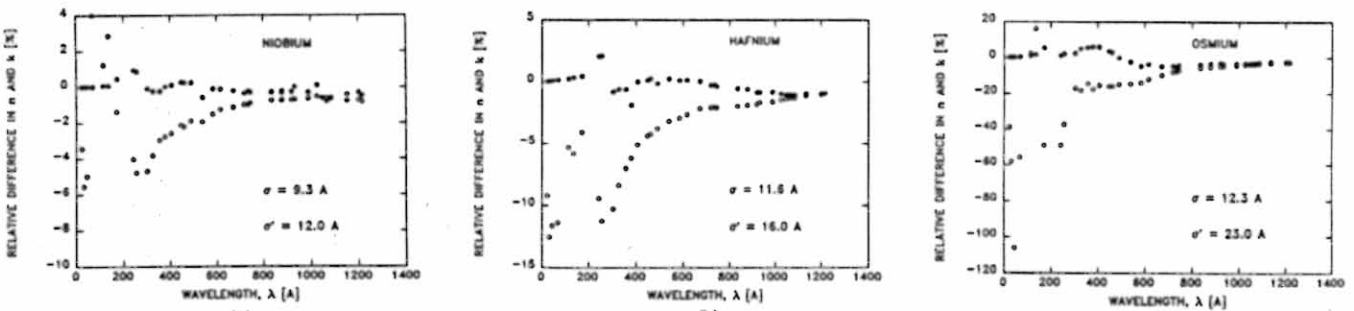

Fig. 6. Relative changes in the derived optical constants, n and k, resulting from two different values of the rms surface roughness, σ and σ', assumed in the determination of the optical constants for three materials. The solid circles correspond to n and the open circles to k: (a) niobium; $\sigma = 9.3$ Å, $\sigma' = 12.0$ Å; (b) hafnium; $\sigma = 11.6$ Å; $\sigma' = 16.0$ Å; (c) osmium; $\sigma = 12.3$ Å, $\sigma' = 23.0$ Å.

Shown in Fig. 6 is the relative difference in the derived optical constants, defined for the index of refraction as

$$\text{relative difference} \equiv \frac{n(\sigma) - n(\sigma')}{n(\sigma)}, \tag{20}$$

with an equivalent expression for the extinction coefficient. The values of σ and σ' are 9.3 Å and 12.0 Å for the niobium data, 11.6 Å and 16.0 Å for the hafnium data, and 12.3 Å and 23.0 Å for the osmium data; so in all cases $\sigma' > \sigma$.

It is clear from Fig. 6 that, in general, the resulting change in the derived extinction coefficient is larger for shorter wavelengths. This is to be expected, as the effect of surface roughness becomes stronger as the wavelength of light approaches the scale of the surface height. We see also that a difference of only a few angstroms in σ can result in a change of several percent

Table V. Optical Constants for CVD SiC

Wavelength (Å)	Index of refraction n		Extinction coefficient k	
23.6	0.99733	(0.99735, 0.99741)	0.000658	(0.000620, 0.000690)
31.6	0.99579	(0.99570, 0.99590)	0.00174	(0.00170, 0.00180)
44.7	0.99387	(0.99385, 0.99405)	0.00346	(0.00323, 0.00350)
67.6	0.9851	(0.9851, 0.9855)	0.0114	(0.0105, 0.0116)
114.0	0.9866	(0.9863, 0.9872)	0.0181	(0.0160, 0.0200)
135.5	0.9791	(0.9788, 0.9794)	0.00433	(0.00400, 0.00470)
171.4	0.9547	(0.9535, 0.9560)	0.0110	(0.0100, 0.0120)
243.0	0.893	(0.892, 0.895)	0.0315	(0.0300, 0.0330)
256.3	0.887	(0.887, 0.889)	0.0339	(0.0325, 0.0355)
303.8	0.854	(0.853, 0.856)	0.0511	(0.0495, 0.0525)
327.0	0.823	(0.821, 0.826)	0.0668	(0.0640, 0.0690)
356.8	0.797	(0.795, 0.800)	0.0909	(0.0860, 0.0940)
379.3	0.776	(0.771, 0.780)	0.117	(0.112, 0.122)
405.9	0.754	(0.750, 0.755)	0.110	(0.106, 0.113)
447.8	0.688	(0.684, 0.688)	0.124	(0.120, 0.128)
460.7	0.664	(0.661, 0.664)	0.130	(0.128, 0.133)
489.5	0.606	(0.602, 0.607)	0.193	(0.187, 0.198)
539.1	0.490	(0.485, 0.493)	0.285	(0.278, 0.293)
584.3	0.401	(0.398, 0.408)	0.520	(0.505, 0.535)
616.3	0.430	(0.420, 0.440)	0.670	(0.635, 0.705)
671.4	0.507	(0.485, 0.530)	0.922	(0.870, 0.970)
718.5	0.562	(0.530, 0.590)	1.09	(1.03, 1.15)
735.9	0.593	(0.550, 0.610)	1.07	(1.04, 1.12)
743.7	0.587	(0.565, 0.610)	1.06	(1.02, 1.10)
834.5	0.719	(0.680, 0.760)	1.27	(1.22, 1.32)
878.0	0.811	(0.760, 0.860)	1.37	(1.32, 1.42)
919.8	0.789	(0.760, 0.820)	1.37	(1.32, 1.42)
932.1	0.754	(0.720, 0.810)	1.33	(1.28, 1.40)
988.8	0.862	(0.810, 0.920)	1.47	(1.41, 1.53)
1025.8	1.00	(0.930, 1.10)	1.65	(1.57, 1.75)
1048.2	0.889	(0.830, 0.950)	1.63	(1.55, 1.67)
1066.7	0.857	(0.800, 0.930)	1.62	(1.54, 1.70)
1085.7	0.974	(0.920, 1.07)	1.69	(1.62, 1.78)
1152.1	0.958	(0.850, 1.10)	1.76	(1.65, 1.88)
1200.7	1.22	(1.10, 1.35)	2.04	(1.94, 2.12)
1215.7	1.26	(1.16, 1.40)	2.10	(2.02, 2.20)

in the derived values of n and k. Conversely, the reflectance calculated from the values of n and k presented in this work may be significantly higher than the actual measured values if surface roughness is ignored in the calculation. This is because the optical constants have been derived using a particular (nonzero) value of σ.

We emphasize that the effect of surface roughness is significant, especially in the soft x rays, and cannot be ignored. We have attempted to characterize surface roughness by optical profilometry. However, the value of σ which results from the optical profilometry measurements will correspond, in general, to a different surface roughness spatial frequency bandwidth than that which is appropriate for the EUV and soft x-ray reflectance measurements. Although the present approach is only approximate, by measuring the surface roughness and including these results in the determination of the optical constants, this source of systematic error has at least been minimized.

IV. Results

The measurements and data reduction techniques just described have thus far been used to derive optical constants for thin films of twenty-one materials. The results for five of these materials are presented in this paper[12]; the optical constants for the remaining sixteen materials are presented in a companion paper.[11]

For each material, the details of the sample preparation are presented; for the e-beam deposited samples this includes sample purity (when available), substrate temperature during deposition, e-beam current, and deposition rate. Also included are the rms surface roughness as determined from the WYKO measurements.

The results of the AES measurements are shown as plots of the peak-to-peak amplitudes of Auger signals of the various elements detected vs sputtering time. For all samples, only carbon, oxygen, and silicon were monitored in addition to the sample material. There may, therefore, be other trace contaminates on some of the samples which were not detected. Sputtering rates, as determined from SiO_2 standards, are included for reference.

The optical constants are presented in both tabular and graphical form. In the graphs, the derived optical constants are presented as discrete points with error bars; some comparisons with data available from the literature are also shown as smooth lines. In the tables, uncertainties in n and k are presented as minimum and maximum values of these quantities.

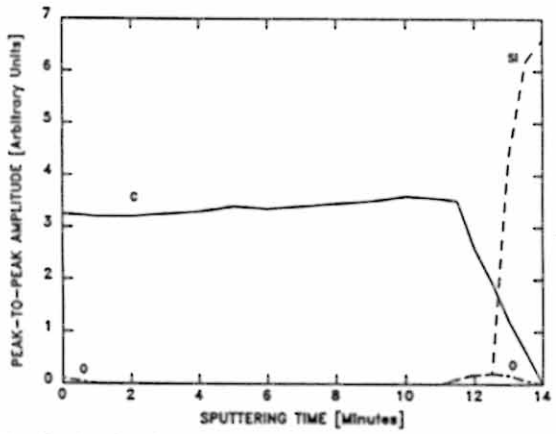

Fig. 7. Peak-to-peak intensity of Auger signal (arbitrary units) vs sputtering time for carbon film.

Also shown for each material are plots of reflectance vs wavelength for six incidence angles—0, 45, 60, 75, 85, and 89°. The reflectance values shown in these graphs were computed from the derived values of the optical constants using the three-phase model described previously and the measured values of the rms surface roughness. No error bars are included. The normal incidence reflectance from 243 Å to 1216 Å is also presented and compared to the reflectance as calculated from values of the optical constants in the literature, where available. Again the reflectances were computed from the values of n and k using the three phase model and the measured surface roughnesses.

A. Carbon

Carbon of unknown purity was evaporated using an e-beam current of 100 mA, which resulted in a deposition rate of 3–5 Å/s. Substrate temperature was kept to under 100°C during deposition. Surface roughness was measured to be 17 ± 4 Å. AES depth profiling was performed with an ion etch rate of 205 ± 14 Å/s. The AES profile, Fig. 7, indicates oxygen at the surface with some oxidation at the Si interface.

The derived optical constants are presented in Fig. 8 and the reflectance in Fig. 9. The reflectance measured in this work is significantly higher than that predicted from the optical constants of Hagemann *et al.*,[13] which are shown for comparison in Fig. 9(b). Hagemann *et al.* determined optical constants from transmission measurements of thin films combined

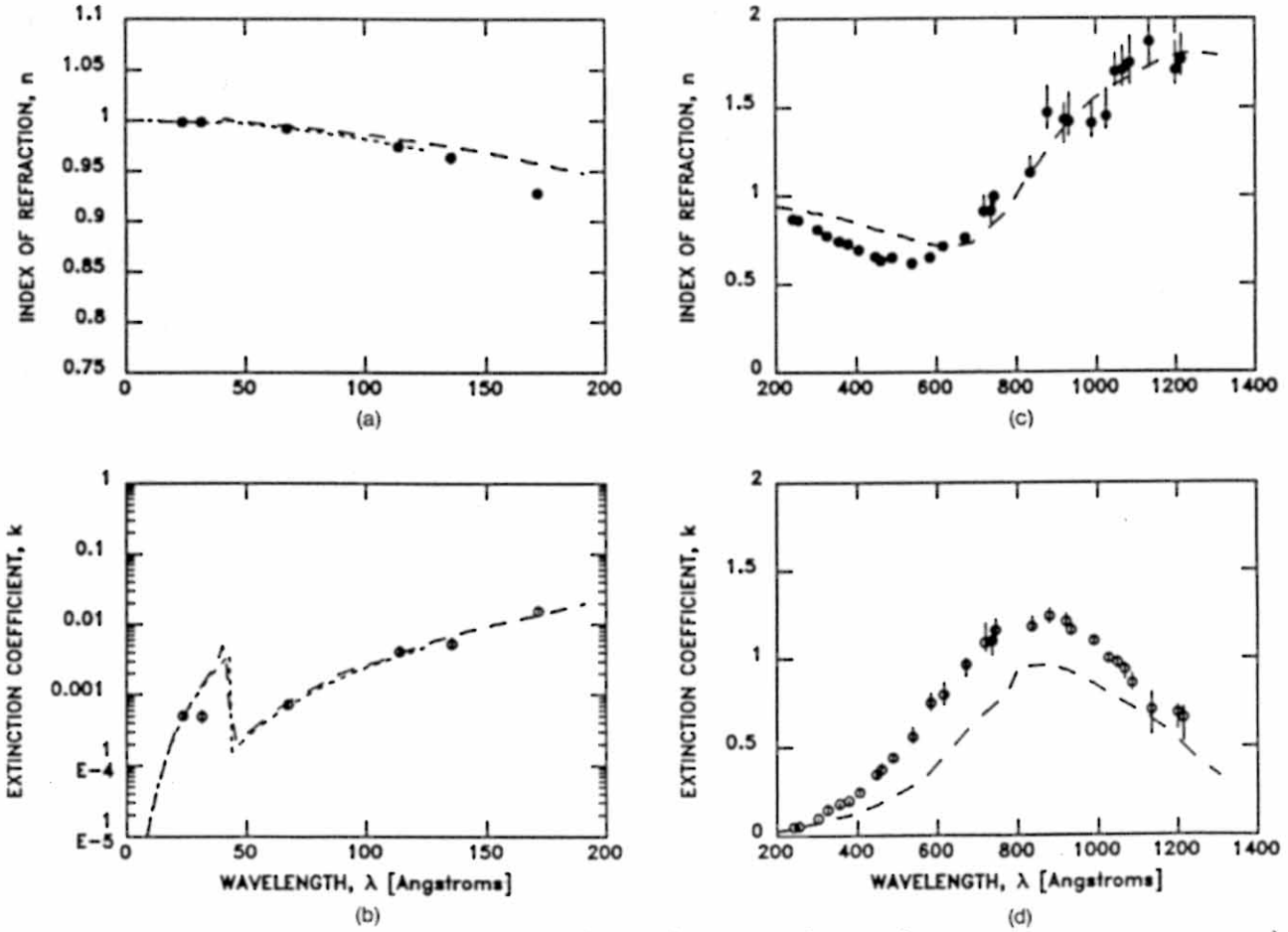

Fig. 8. Index of refraction for carbon vs wavelength from (a) 0 Å to 200 Å and (b) 200 Å to 1400 Å and extinction coefficient from (c) 0 Å to 200 Å and (d) 200 Å to 1400 Å. Shown also are the data of Henke *et al.*[14] (short dashed line) and of Hagemann *et al.*[13] (long dashed line).

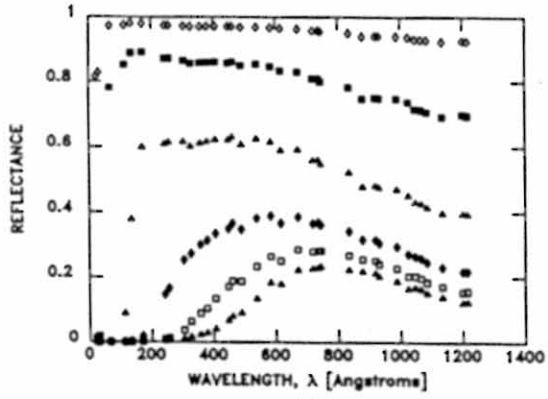

Fig. 9. (a) Reflectance of carbon vs wavelength at six incidence angles: 0, 45, 60, 75, 85, and 89°. (b) Normal incidence reflectance vs wavelength. The data of Hagemann *et al.*[13] are shown for comparison in (b).

with Kramers-Kronig analysis. Also shown for comparison are the data of Henke *et al.*[14] In the short-wavelength region, the index of refraction data agrees somewhat better with the data of Henke *et al.* than with Hagemann *et al.* In the long-wavelength region, the shape of the curves is in general agreement with the data of Hagemann *et al.*, but the broad minimum in n occurs at a wavelength of ~550 Å rather than at ~700 Å as given by Hagemann *et al.*

B. Synthetic Diamond

Diamond is a material of considerable interest in the present wavelength region. Measurements performed on bulk samples (see Palik[8] and references therein) indicate a normal incidence reflectance of more than 60% near 1000 Å. Unlike aluminum and silicon, however, which have even higher reflectances in this range, diamond is presumably unaffected by exposure to air. Recently, the technology to fabricate synthetic diamond films has been developed (see, for example, Sawabe and Inuzuka[1] and Ono *et al.*[15]). Applications for such films in the EUV would include coatings for front surface mirrors and gratings.

The diamond film measured in this work did not appear uniform; interference effects in visible light were obvious, as were minute fractures near the edges of the sample. Also, when the sample was aligned in the reflectometer with laser light, it was found that the surface was not uniformly flat, although it was rather smooth; surface roughness measurements indicated an rms surface roughness of 10 ± 1 Å. The departure from a perfectly flat surface, however, may be due to the flexibility of the thin Si substrate rather than a problem with the film. The surface roughness measurements were performed on the sample with and without an overcoating of aluminum (to ensure opacity for the optical interferometry), and the roughness was essentially the same in both cases.

The nonuniformity visible to the eye was also apparent in the EUV reflectance, which varied considerably across the surface. A small spot of ~5 mm in diameter was found to have the highest normal incidence reflectance at 1048 Å, and this spot was, therefore, selected for further reflectance measurements. Auger depth profiling measurements were not performed on the diamond sample. However, SEM measurements performed at LANL suggested a film thickness of the order of 1 μm. X-ray diffraction measurements, also performed at LANL, verified the diamond structure of the film.

Due to the nonuniformity of the sample surface, reflectance measurements were not possible below 200 Å. At these wavelengths, reflectance measurements must be made near grazing incidence. But such large incidence angles require illumination of a larger area of the surface. Since the surface was considerably nonuniform, measurements at different incidence angles sampled different parts of the surface and were, therefore, unreliable.

The optical constants are shown in Fig. 10 and the reflectance in Fig. 11. Shown for comparison are the data of Philipp and Taft.[16] Philipp and Taft measured the normal incidence reflectance of bulk diamond and used Kramers-Kronig analysis to derive optical constants.

The optical constants shown in Fig. 10 do not agree at all with the results of Philipp and Taft, and the normal incidence reflectance [Fig. 11(b)] is much lower than that given by Philipp and Taft for bulk diamond. The lower reflectance for the present sample is disappointing, but one must bear in mind that measurements were made on only one sample, and this sample was highly nonuniform; the possibility of fabricating high-reflectance diamond films should not be ruled out.

C. Aluminum

Aluminum of unknown purity was evaporated using an e-beam current of 300 mA, resulting in a deposition rate of 20–25 Å/s. The substrate was held to room temperature during deposition. Surface roughness was measured to be 21.3 ± 3 Å. Aluminum is known to rapidly form an oxide layer of the order of 40 Å thick. The sample measured here also has oxidized. The AES profile shown in Fig. 12 indicates oxidation and carbon contamination essentially confined to the sur-

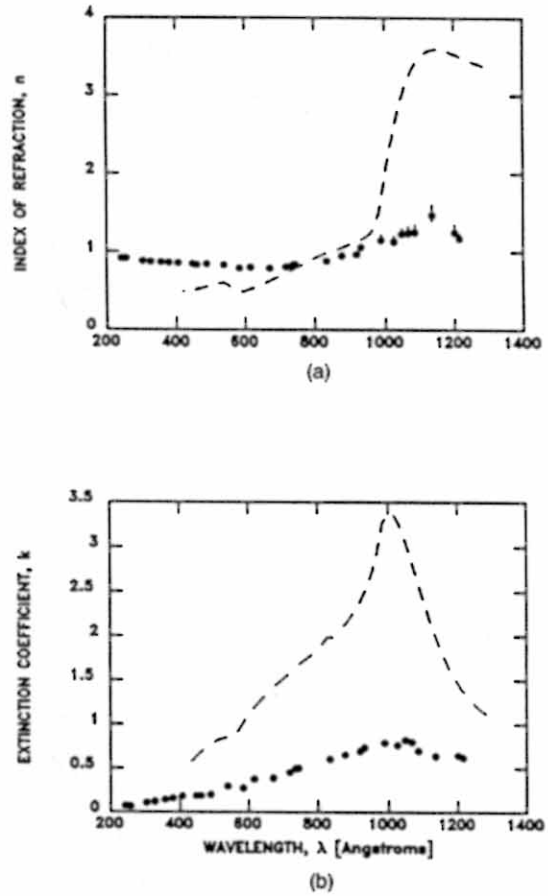

Fig. 10. Index of refraction for synthetic diamond film vs wavelength from (a) 200 Å to 1400 Å and extinction coefficient from (b) 200 Å to 1400 Å. Shown also are the data of Philipp and Taft[16] (dashes).

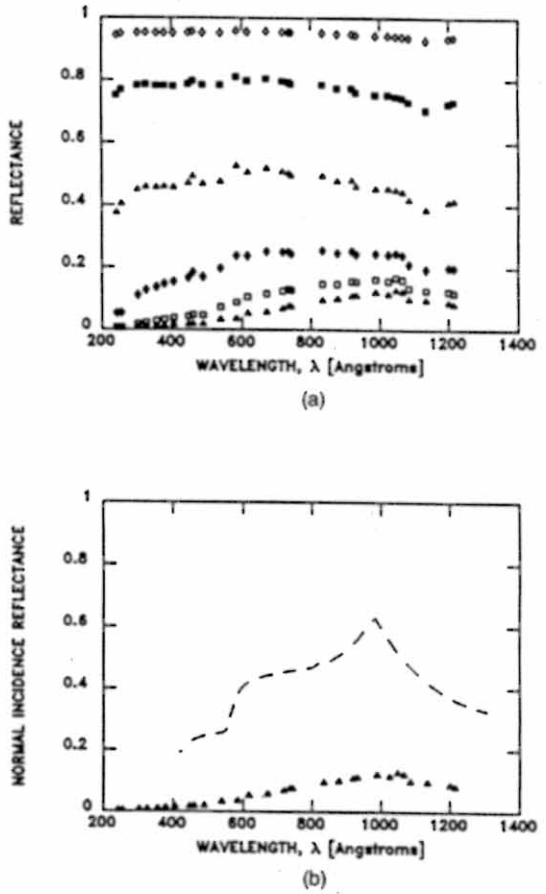

Fig. 11. (a) Reflectance of synthetic diamond film vs wavelength at six incidence angles: 0, 45, 60, 75, 85, and 89°. (b) Normal incidence reflectance vs wavelength. The data of Philip and Taft[16] (dashes) are shown for comparison.

face of the film and oxidation at the Si interface. Ion etching was performed with a sputtering rate of 176.5 ± 8.6 Å/min.

The optical constants are shown in Fig. 13 and the reflectance in Fig. 14. Shown for comparison are the data of Henke *et al.*[14] and Shiles *et al.*,[17] which were taken from Palik.[8] Also shown are the data for Al_2O_3 of Henke *et al.* and Hagemann *et al.*[13] The data of Shiles *et al.* were determined from data taken from many sources combined with Kramers-Kronig analysis. Hagemann *et al.* measured the transmission of thin films and also used Kramers-Kronig analysis to derive optical constants.

From Fig. 14(b), it is apparent that the normal incidence reflectance is lower than that reported by both Shiles *et al.* for Al and Hagemann *et al.* for Al_2O_3. In Fig. 13, the *L*-absorption edge of Al is visible in the extinction coefficient at 170 Å and appears as a pimple in the index of refraction. The data for n and k agree well with those of Shiles *et al.* below ~500 Å. Above 500 Å, there is significant departure from the data for both Al and Al_2O_3.

D. Silicon

Silicon of 99.999% purity was evaporated using an e-beam current of 75 mA, resulting in a deposition rate of 3–7 Å/s. The substrate temperature was kept to 75°C during deposition. Surface roughness was measured to be 18.7 ± 2.5 Å. The AES profile shown in Fig. 15 indicates the presence of oxygen and carbon throughout the film. Ion etching was performed with a sputtering rate of 178.4 ± 4.7 Å/min.

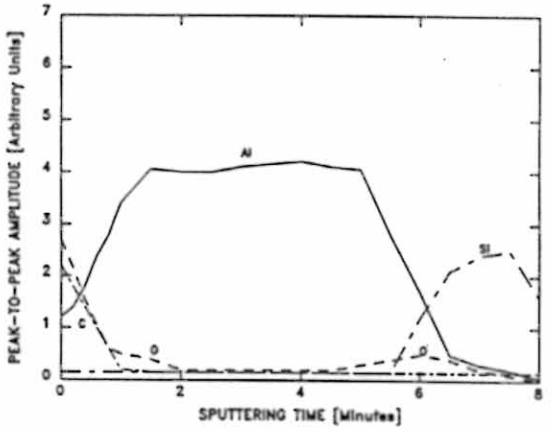

Fig. 12. Peak-to-peak intensity of Auger signal (arbitrary units) vs sputtering time for aluminum film.

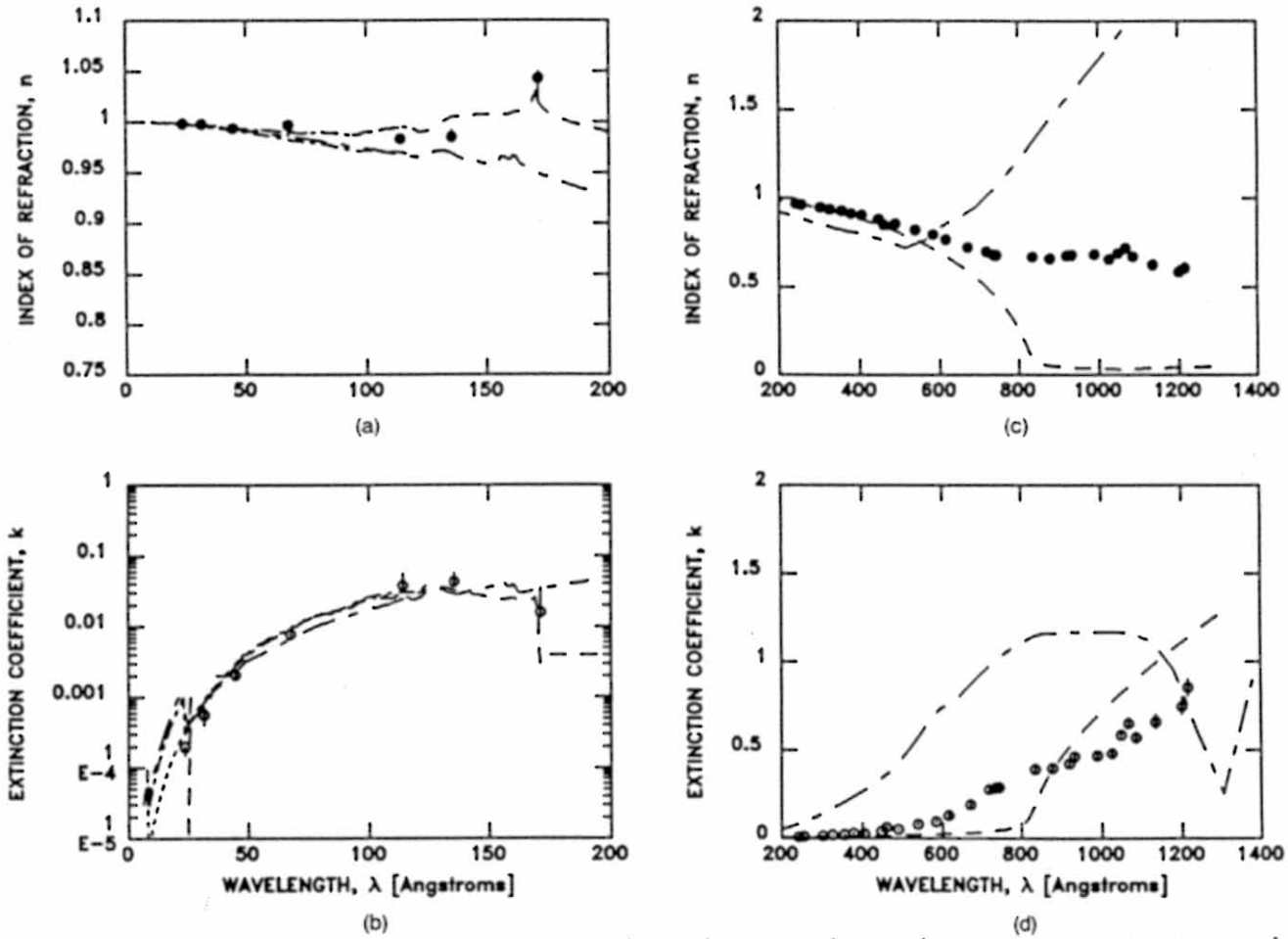

Fig. 13. Index of refraction for aluminum vs wavelength from (a) 0 Å to 200 Å and (b) 200 Å to 1400 Å and extinction coefficient from (c) 0 Å to 200 Å and (d) 200 Å to 1400 Å. Shown also are the data of Henke *et al.*[14] for Al (dot) and Al_2O_3 (dot–dash), Shiles *et al.*[17] for Al (dashes), and Hagemann *et al.*[13] for Al_2O_3 (dot–long dash).

The optical constants are shown in Fig. 16 and the reflectance in Fig. 17. Shown for comparison are the data for silicon of Henke *et al.*[14] and the data taken from Palik[8] for both crystalline and amorphous Si. Also shown are the data for SiO_2 of Henke *et al.* and the data of Palik for crystalline and amorphous SiO_2.

In the short-wavelength region, the data agree better with those for SiO_2 than with Si. The feature at 123 Å is the L-absorption edge in Si, and that at 23 Å in the SiO_2 data is the K-absorption edge in O. At the longer wavelength, the normal incidence reflectance is lower for most wavelengths than that given by the data taken from Palik for both Si and SiO_2. The optical data show essentially none of the sharp features apparent in the SiO_2 data nor do they agree well with the data for Si, for wavelengths >600 Å.

E. CVD Silicon Carbide

Silicon carbide is well known for its high reflectance in the EUV. Its optical properties combined with its desirable thermal and mechanical properties make it particularly attractive for use in synchrotron and space astronomy instrumentation.

The details of the sample fabrication for the SiC sample measured in this work can be found in Takacs.[18] Unlike the other samples measured in this work, the SiC sample was precleaned prior to reflectance measurements. Following the procedure outlined by Rehn *et al.*,[19] the sample was heated to 70°C for 30 min and then etched in concentrated HF before being transferred in air to the reflectometer. Surface roughness measurements indicated an rms surface roughness of 15 ± 1 Å. Auger depth profiling measurements were not performed on the CVD SiC sample.

The optical constants are shown in Fig. 18 and the reflectance in Fig. 19. Shown for comparison are the data of Henke *et al.*,[14] Osantowski,[20] and Rehn *et al.*[19] and Leveque and Lynch (unpublished) which were taken from Palik.[8]

The normal incidence reflectance [Fig. 19(b)] is close to that given by the data taken from Palik, but for wavelengths >600 Å the reflectance is not quite as high. The optical constants agree very well with those given by both Henke *et al.* and Osantowski, but the index of refraction departs from the data of Palik

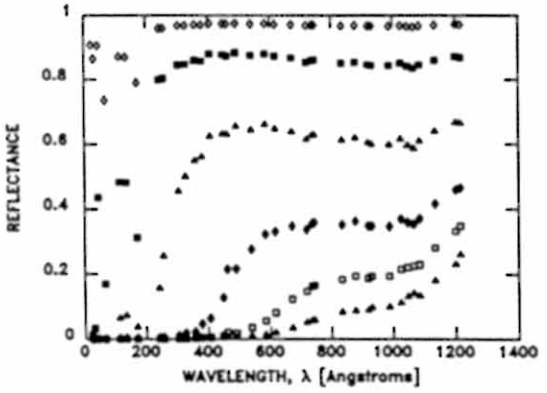

Fig. 14. (a) Reflectance of aluminum vs wavelength at six incidence angles: 0, 45, 60, 75, 85, and 89°. (b) Normal incidence reflectance vs wavelength. The data of Shiles *et al.*[17] for Al (dash) and of Hagemann *et al.*[13] for Al_2O_3 (dot-long dash) are shown for comparison.

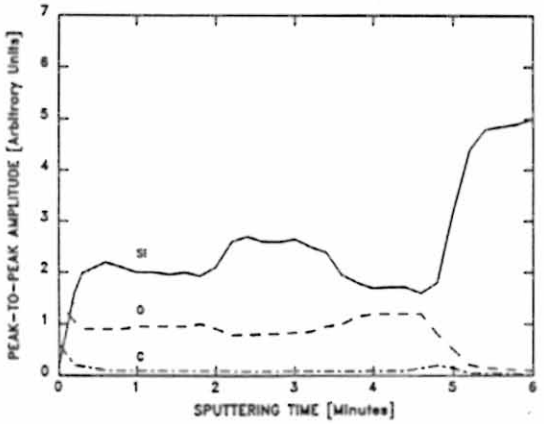

Fig. 15. Peak-to-peak intensity of Auger signal (arbitrary units) vs sputtering time for silicon film.

above 600 Å. The silicon L-absorption edge is visible in the extinction coefficient near 123 Å. The only other significant feature in the data is the dip in the index of refraction curve near 600 Å.

V. Conclusion

A nonlinear least-squares curve-fitting technique based on the χ^2 test has been applied to the derivation of optical constants from reflectance vs angle of incidence measurements. The technique incorporates independently measured values of the film surface roughness, film thickness, and incident beam polarization. Additionally, probable errors in the derived optical constants can be estimated directly by evaluating confidence intervals in parameter space, as described in Sec. III.

The curve-fitting technique was used to derive optical constants for thin film samples from reflectance vs angle of incidence measurements using a computer-controlled reflectometer. The optical constants for samples of C, diamond, Al, Si, and CVD SiC have been presented in this paper; optical data for sixteen metals are presented in a companion paper. Auger electron spectroscopy depth profiling measurements were used to evaluate sample composition including oxidation and contamination.

The differences between the present results and data taken from the literature can be explained in part by genuine sample differences, although some of the results may not agree because of differences in data reduction techniques. It is clear from the AES depth profiling measurements that the Si and Al samples are highly oxidized. The optical data for these two samples are, therefore, inappropriate for UHV coating applications. The determination of the optical constants for UHV prepared films of these and other materials using the present techniques would require an ultrahigh-vacuum reflectometer preferably with in situ deposition and AES capabilities. Additionally, possible future work would be performed using synchrotron radiation so as to provide better energy resolution and also include measurements of the sample crystallinity.

The optical constants presented in this work were determined assuming particular values of the surface height σ. The reflectance calculated using the values of n and k thus presented will be higher than that actually measured, especially for the shorter wavelengths, unless the surface roughness is included in the calculation using the Debye-Waller factor in the Fresnel reflection coefficients. Surface roughness is an important parameter in the EUV and soft x rays and should not be ignored; although the method presented here to account for surface roughness is only approximate, the systematic error which would otherwise result in the derivation of the optical constants has been minimized.

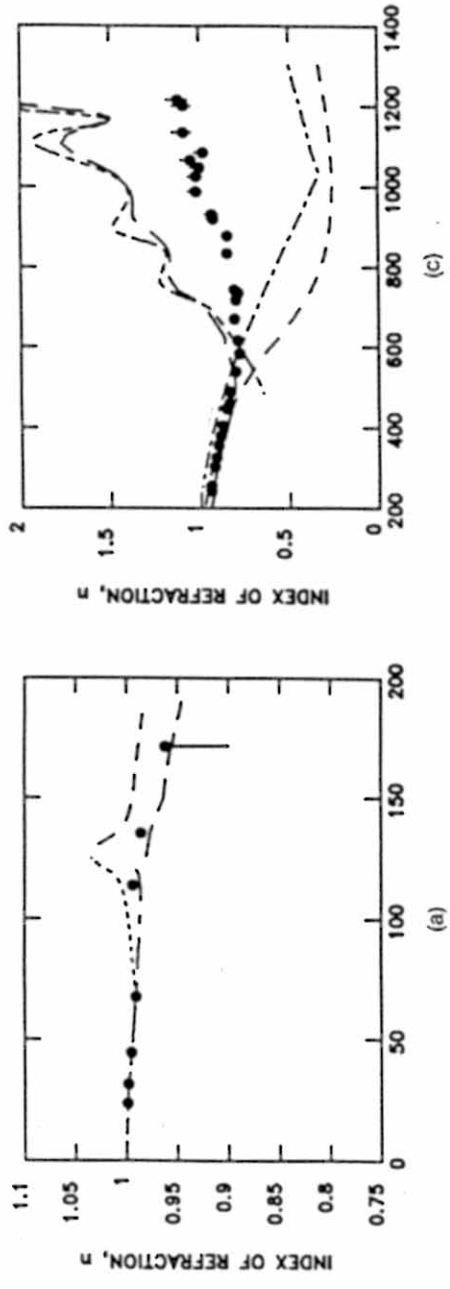

Fig. 16. Index of refraction for silicon vs wavelength from (a) 0 Å to 200 Å and (b) 200 Å to 1400 Å and extinction coefficient from (c) 0 Å to 200 Å and (d) 200 Å to 1400 Å. Shown also are the data for Si (dots) and SiO_2 (dot–long dash) of Henke *et al.*[14] and the data on crystalline Si (dashes), amorphous Si (dot–dash), crystalline SiO_2 (dot–dot–dot–dash), and amorphous SiO_2 (long dash), all taken from Palik.[8]

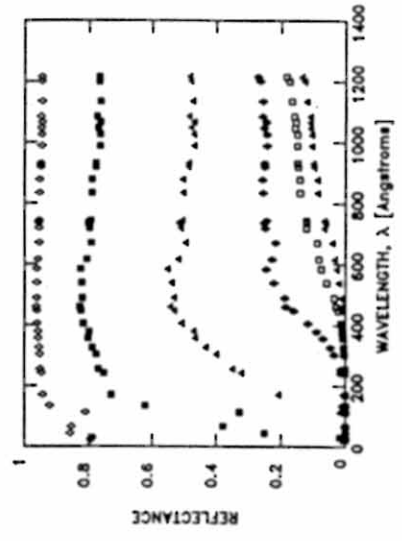

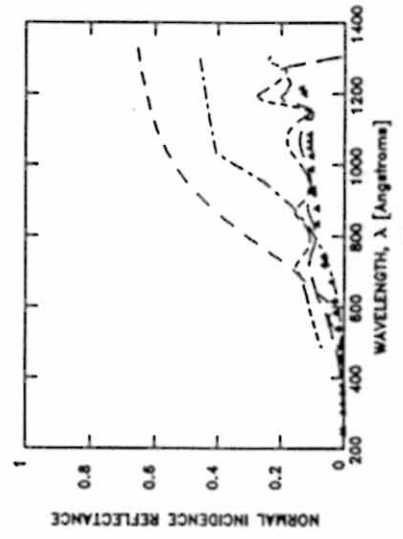

Fig. 17. (a) Reflectance of silicon vs wavelength at six incidence angles: 0, 45, 60, 75, 85, and 89°. (b) Normal incidence reflectance vs wavelength. The data on crystalline Si (dash), amorphous Si (dot–dash), crystalline SiO_2 (dot–dot–dot–dash), and amorphous SiO_2 (long dash), all taken from Palik,[8] are shown for comparison.

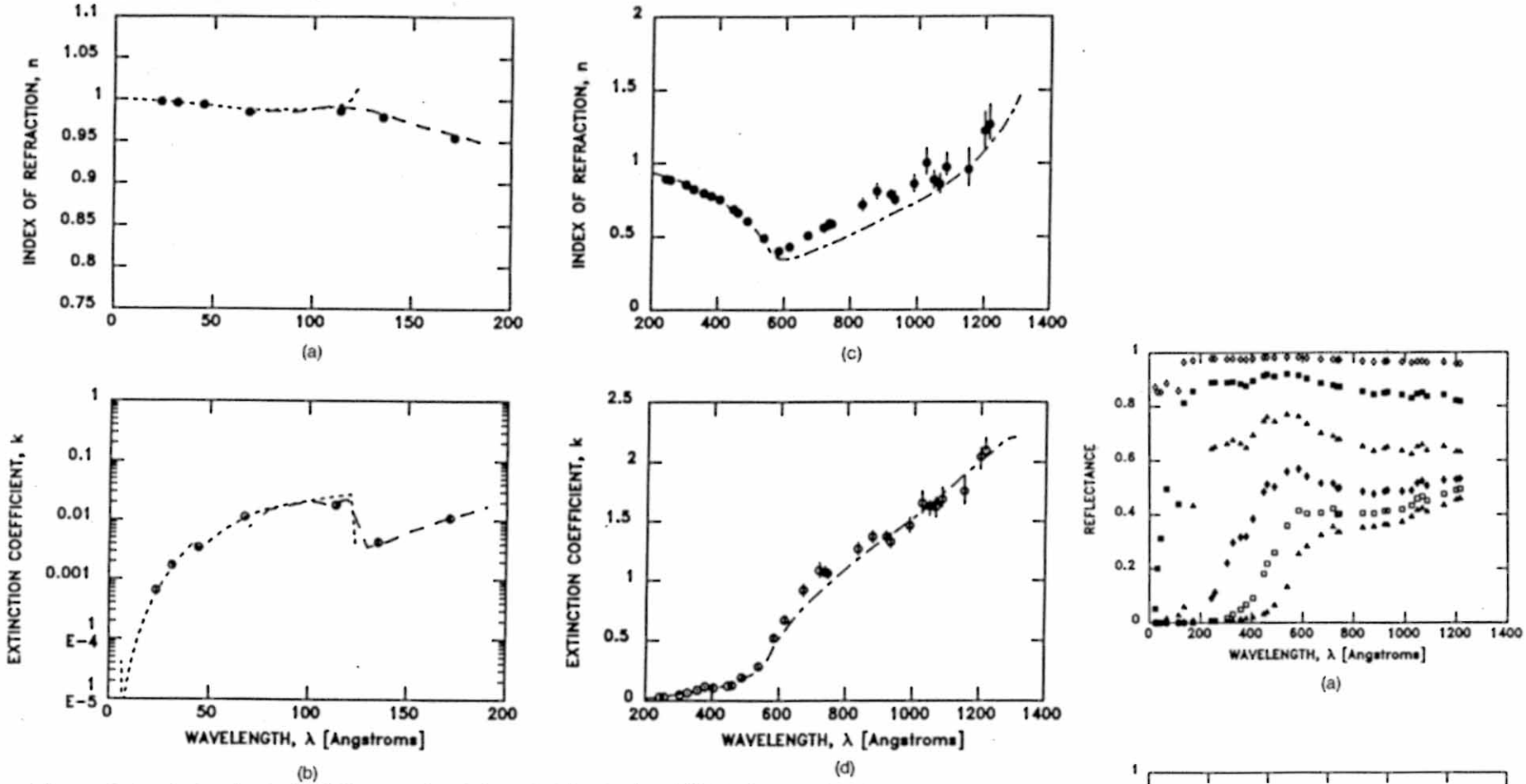

Fig. 18. Index of refraction for CVD SiC vs wavelength from (a) 0 Å to 200 Å and (b) 200 Å to 1400 Å and extinction coefficient from (c) 0 Å to 200 Å and (d) 200 Å to 1400 Å. Shown also are the data of Henke *et al.*[14] (dots), Osantowski[20] (dashes), and Palik[8] (dot–dash).

Fig. 19. (a) Reflectance of CVD SiC vs wavelength at six incidence angles: 0, 45, 60, 75, 85, and 89°. (b) Normal incidence reflectance vs wavelength. The data of Palik[8] (dot–dash) are shown for comparison.

This work was sponsored in part by NASA grants NAG 5-96 and NSG 5303, DOE contract W-7405-ENG-36, and Los Alamos National Laboratory institutionally sponsored research and development funds.

David L. Windt is presently with the Lockheed Palo Alto Research Laboratory, Palo Alto, CA.

References

1. A. Sawabe and T. Inuzuka, "Growth of Diamond Thin Films by Electron Assisted Chemical Vapor Deposition," Appl. Phys. Lett. **46**, 146 (1985).
2. D. L. Windt and W. Cash, "The Soft X-Ray/EUV Calibration Facility at the University of Colorado," Proc. Soc. Photo-Opt. Instrum. Eng. **689**, 167 (1986).
3. D. L. Windt, "The Optical Properties of 21 Thin Film Materials in the 10 eV to 500 eV Photon Energy Region," Ph.D. Thesis, U. Colorado (1987) (unpublished).
4. B. Bhushan, J. C. Wyant, and C. L. Koliopoulus, "Measurement of the Surface Topography of Magnetic Tapes by Mirau Interferometry," Appl. Opt. **24**, 1489 (1985).
5. K. Rabinovitch, L. R. Canfield, and R. P. Madden, "A Method for Measuring Polarization in the Vacuum Ultraviolet," Appl. Opt. **4**, 1005 (1965).
6. The reflectance measurements and polarization measurements presented in this work cannot distinguish between circularly polarized light and unpolarized light. The unpolarized component of the incident beam may, therefore, contain a circularly polarized component (which is irrelevant to this work), and hence this description of the polarization of the incident beam is not entirely accurate.
7. The reflectance vs angle of incidence of the rhodium mirror analyzer was measured as a function of wavelength, and the results were found to agree well with the data given by Palik.[8]
8. E. D. Palik, *Handbook of Optical Constants of Solids*, E. D. Palik, Ed. (Academic, Orlando, 1985).
9. P. R. Bevington, *Data Reduction and Error Analysis for the Physical Sciences* (McGraw-Hill, New York, 1969).
10. M. Lampton, B. Margon, and S. Bowyer, "Parameter Estimation in X-ray Astronomy," Astrophys. J. **208**, 177 (1976).
11. D. L. Windt, W. C. Cash, Jr., M. Scott, P. Arendt, B. Newnam, R. F. Fisher, and A. B. Swartzlander, "Optical Constants for Thin Films of Ti, Zr, Nb, Mo, Ru, Rh, Pd, Ag, Hf, Ta, W, Re, Os, Ir, Pt, and Au from 24 Å to 1216 Å, Appl. Opt. **27**, 000 (15 Jan. 1988).
12. The entire set of optical constants as well as related optical functions and a more detailed account of the measurement and data reduction techniques are in Ref. 3.
13. H. J. Hagemann, W. Gudat, and C. Kunz, "Optical Constants from the Far Infrared to the X-Ray Region: Mg, Al, Cu, Ag, Au, Bi, C, and Al_2O_3," DESY Report SR-74/7, Hamburg (1974).
14. B. L. Henke, P. Lee, T. J. Tanaka, R. L. Shimabukuro, and B. K. Fujikawa, "The Atomic Scattering Factor, $f_1 + if_2$, for 94 elements and for the 100 to 2000 eV Photon Energy Region," AIP Conf. Proc. **75**, 340 (1981).
15. A. Ono, T. Baba, H. Funamoto, and A. Nishikawa, "Thermal Conductivity of Diamond Films Synthesized by Microwave Plasma CVD," Jpn. J. Appl. Phys. **25**, L808 (1986).
16. H. R. Philipp and E. A. Taft, "Optical Properties of Diamond in the Vacuum Ultraviolet," Phys. Rev. **127**, 159 (1962).
17. E. Shiles, T. Sasaki, M. Inokuti, and D. Y. Smith, "Self-consistency and Sum-Rule Tests in the Kramers-Kronig Analysis of Optical Data: Applications to Aluminum," Phys. Rev. B **22**, 1612 (1980).
18. P. Z. Takacs, "Evaluation of CVD Silicon Carbide for Synchrotron Radiation Mirrors," Nucl. Instrum. Methods **195** (1/2), 259 (1982).
19. V. Rehn, J. L. Stanford, and V. O. Jones, in *Proceedings, Thirteenth International Conference on Physics and Semiconductors*, Rome, 1976, F. G. Fumi, Ed. (Typografia Marves, Rome, 1976), p. 985.
20. J. Osantowski, data presented at the Glancing Incidence Optics Fabrication Workshop, hosted by the Optics Branch of the Goddard Space Flight Center, Annapolis, MD, 1–4 Apr. 1985.